

Motion tracking in MRI by Harmonic State Model: Case of heart left ventricle

P. Lionel EVINA EKOMBO

*Informatics Statistics & Quality Laboratory
Dhar Mehraz Sciences Faculty
Sidi Mohammed Ben Abdellah University
Fes, Morocco*

evinalio@yahoo.fr

Mohammed OUMSIS

*Informatics Statistics & Quality Laboratory
Dhar Mehraz Sciences Faculty
Sidi Mohammed Ben Abdellah University
Fes, Morocco*

oumsis@fsdmfes.ac.ma

Mohammed MEKNASSI

*Informatics Statistics & Quality Laboratory
Dhar Mehraz Sciences Faculty
Sidi Mohammed Ben Abdellah University
Fes, Morocco*

m.meknassi@gmail.com

Abstract

We have developed a new method for tracking the closed contour which is based on a harmonic state model (HSM). It tracks the heart's left ventricle (LV) throughout cardiac cycle. This method provides trajectories of points about the contour of the LV, crucial information in cardiac motion analysis. The state vector associated with HSM provides a robust and accurate modeling of contour closed. We rely on the state vector and we use it as local descriptor of region of the LV. This local description enables us to obtain the characteristic points of the contour. Owing the fact that, only light movements between cycle's instants exists. The mapping of these points by the LCSS is relevant. The repetition of this process allows us to build LV trajectories, but also, for further information on its movement, bull eye graphs. The application of the simulation method gives the best results. The same is true on 2D plans sequences extracted from real cine-MRI volume. The trajectories calculated, the generated graphics, allow us to easily observe the difference between a healthy and a sick heart.

Keywords: Harmonic State Model, tracking movement, LCSS, cardiac imagery, MRI.

1. INTRODUCTION

According to the World Health Organization, cardiovascular diseases are a leading cause of death in the world. Thus cardiac function estimation is a main interest. It is useful for the various stages: diagnosis, therapy and intervention. The relevance of the diagnosis is connected to the appreciation of the nature, location and extent of the lesion. The cardiac anomalies affect, according to the cases, the rhythm, the perfusion, the contraction or the metabolism of the heart

carried out by the myocardium. It is not only important to detect diseases, but also to evaluate its effect on cardiac structure. This is done by tracking the volumes of cardiac chambers, thickness and movement of the walls of the myocardium. Much of these anomalies are due to a disturbance of the myocardial contractile function, particularly the left ventricle (LV). Tracking of left ventricular movement allows the detection of many cardiovascular diseases. Medical imaging provides essential support for cardiac diagnosis. It provides morphological information (shape, dimensions and volume), dynamic (motion, deformation, speed) and functional (perfusion, metabolic activity). Magnetic Resonance Imaging (MRI), which is non-invasive, allows a complete sight quality of the morphology of the LV. The accuracy of the measurements from the MRI images is demonstrated at [1]. It testifies MRI as the best source for the image analysis of LV. However, extraction of these measures is not helped by the weakness of the resolution and the presence of noise. It can be done either implicitly or explicitly. In the first case, a clinician relying on his job experience can mentally imagine the dynamic behavior of the heart and draw a diagnosis from it. Therefore, one can observe a great variability inter-and intra-observer. In the second case, it is the field of numerical methods through the use of modeling techniques spatiotemporal, excellent modeling alternative, which provides many parameters for the analysis. This employment is done in three stages: segmentation of the LV contour from cardiac images and modeling (2D/3D) the LV pattern, temporal tracking of the LV movements and finally the analysis of calculated parameters in the two previous steps for the issue of diagnosis. In this article a great interest is carried on the second stage of the spatiotemporal modeling, in occurrence the tracking. Tracking the LV movement is a key stage in the process of analysis of cardiac sequences. It provides crucial information on the temporal evolution of LV and at the same time on the state of the heart.

A lot of work has been made, but there are still gaps particularly in terms of accuracy. It also remains costly to implement it in medical software in hospitals. The accuracy of tracking obtained by cardiac MRI-tagged [2, 3] is not matched by these methods. The MRI-tagged does not cover the entire cardiac cycle: it is due to the reabsorbed liquid contrast. This makes it inapt for wide clinical use. The Echocardiography is one of the emerging diagnostic tools for visualizing cardiac structure. It allows diagnosing cardiovascular diseases. Ultrasound imaging is real-time, noninvasive and less expensive than CT and MR. Unfortunately, However, the low signal-to-noise ratio and the multiplicative nature of the noise corrupting the ultrasound images. Then, we have poor object boundaries and make the LV segmentation a difficult task. These images require pretreatment before any use. In [4], authors combine an edge preserving total variation based denoising algorithm and a robust tracker [5]. This process is efficient but stays complex and need a large number of images. In [6], authors use derivatives filters to upgrade grayscale image and it gives good resultants which we could use.

The objective of this speech is to present a new approach relying on both precision and speed in tracking the left ventricle. It is specifically designed to this shape. It is based on a Harmonic State Model (HSM) [7]. This model provides a good modeling of a closed contour (a periodic evolution) and has a robust state vector which exploits the Kalman filter for estimation.

In [7], we proposed a modeling of cardiac motion (left ventricular movement) by a model state harmonic and linear. This motion model combines three essential characteristics of the ventricular movement namely: - access to cardiac dynamics over the whole cycle, - unquestionable robustness to noises, - and direct physical interpretation of functional parameters of LV. The model is linear, periodic and reflects a dynamic model of the decomposition in Fourier series of the cardiac motion. Used as a model state in a Kalman filter, this model offers the advantage of providing an estimate robust to noises, movement parameters such as speed and acceleration which are components of the vector state model. So far, the Harmonic State Model (HSM) has been used in a temporal dimension to model the movement of the LV. The periodicity of the shape of LV (closed surface) also allows us to transpose the model into a spatial dimension. This is enabled with the introduction of shape constraints and smoothness via the harmonic decomposition. This double feature displays the potential of such a model for tracking of 2D/3D wall LV in a sequence of images. We will, therefore, an application of the model HSM in a spatial dimension to model the contours of the LV in order to track local deformations of the regions of LV. In others works, we see that we could use this model in retrieval image system following steps defined in those works [8], [9] and [10].

This paper is divided into four parts. First of all, we will present a state of the art, the HSM model and our tracking method. Then a simulation will be made with data to evaluate our approach, followed by an implementation of real patients' data. Finally, we will draw a conclusion and some perspectives.

2. DESCRIPTION OF THE METHOD

2.1 State of art

Many studies have been conducted to provide tools of assistance to the diagnosis. These works range from the heart segmentation in image sequences to its analysis, through the modeling of shape and track the movement of the heart. Research on tracking can be divided into two groups depending on the type of movement approach: rigid and not-rigid. The movement of the LV is a not-rigid one. Active contours proposed by Kass and al. [11] ensure this type of tracking and the work arising around. Nevertheless, they are sensitive to the information. They do not include details related to the LV shape, for example, the periodicity of LV, and the cyclic aspect of cardiac motion. The boundary of active contours is their sensitivity to initial positions [12]. Shift methods provide interesting results, but it requires mostly temporal rather complex [13, 14]. The Iterative Closest Point (ICP) presented by Besle and Mc Kay [15] is a method also very much used for tracking. Improved versions are constantly being made; they include the extent of matching (distance measurement, optical flow, etc.) [16], [17], [18]. Others versions are based on the transformation functions (rigid or not-rigid) [18], [19]. We can also mention the algorithms based on optical flow. These optical flow algorithms provide important information for motion analysis of image sequences by attempting to find the vector field which describes spatial movements of image objects over time. Different methods for computation of optical flow can be classified in three main categories: feature-based, gradient-based and correlation-based. [20] gives more details about it. The 2D tracking algorithms are widely presented in [21], [22]. Yilmaz [21] shows that tracking of objects has two phases. The first phase is detection of objects which includes 4 types of algorithms:

- the detection of points that mark points of interest of an image (Harris, KLT, ASG);
- the subtraction of background which constructs a model of representation of the scene;
- segmentation which partitions the image into regions similar (Mean Shift);
- supervised learning that builds a function for mapping data with the expected output (adaptive boosting, SVM).

The second phase, which is the most critical, is the mapping of instances of the object. It includes several families of algorithms:

- filtering that allows the mapping of points of interest from one image to another (particle filters, Kalman filter);
- the tracking body that uses coded information to inside the object region;
- the tracking by kernel research subject compared to a model built in the previous images.

The problem of automatic detection and segmentation of heart volumes have received considerable attentions [23], [24]. In papers [25] and [26], tracking of the left ventricles (LV) have particular attracted interests. It provides clinical significance for specialists to evaluate disease.

Beyond this work, our attention has been drawn by methods which measure distances give good results; it is specifically the work of Wang [27], Papademetris [28] and Geiger [29].

In this document, we propose a new method to estimate the not-rigid motion that would fill the gaps identified in the methods mentioned. In addition to that, it generates the trajectories of the control points of the LV during the cardiac cycle, as well as parameters allowing a classification of the patient as being healthy or pathological. Our method takes into account the periodicity contour of LV and operates through the HSM. It should be noted that the HSM [7] has been used for modeling the temporal movement of the LV (periodic motion). This model is also reducing the impact of noise measures by carrying out a filtering of data through the Kalman filter.

2.2 State Harmonic Decomposition of periodic function

Let $s(t)$ be a periodic continuous signal (2D coordinates of a curve for example), $s(t)$ harmonic decomposition truncated at level n is:

$$s_n(t) = \bar{s} + A_1 \sin(\omega t + \varphi_1) + \dots + A_n \sin(n\omega t + \varphi_n) \quad (1)$$

Where $s_n(t)$ is the truncated Fourier series at order n . $A_1 \dots A_n$ are weighting coefficients, ω is the pulsation and $\varphi_1 \dots \varphi_n$ the phases.

Our goal is to find a discrete linear state model according to equation:

$$\begin{cases} S_n(k+1) = F S_n(k) + \zeta(k) \\ s_n(k) = H S_n(k) + \xi(k) \end{cases} \quad (2)$$

where k is the discrete variable ($s_n(k) = s_n(k\Delta T)$, ΔT the sampling period), $S_n(k)$ is the state vector at index k , F is the transition matrix, H is the measurement matrix and $\zeta(k)$ and $\xi(k)$ are zero mean Gaussian noises of covariance matrix respectively $Q(k)$ and $R(k)$.

2.2.1 Choice of a state vector

For sample $k+1$ corresponding to $t+\Delta t$, the truncated harmonic decomposition is, according to equation (1):

$$\begin{aligned} s_n(k+1) &= s_n(t + \Delta t) \\ &= \bar{s} + A_1 \sin(\omega(t + \Delta t) + \varphi_1) + \dots + A_n \sin(n\omega(t + \Delta t) + \varphi_n) \end{aligned} \quad (3)$$

By developing:

$$\begin{aligned} s_n(t + \Delta t) &= \bar{s} + A_1 \sin(\omega t + \varphi_1) \cos(\omega \Delta t) + A_1 \cos(\omega t + \varphi_1) \sin(\omega \Delta t) + \dots \\ &+ A_n \sin(n\omega t + \varphi_n) \cos(n\omega \Delta t) + A_n \cos(n\omega t + \varphi_n) \sin(n\omega \Delta t) \end{aligned} \quad (4)$$

Our goal is to find a state vector $S_n(t)$ including $s_n(t)$ and its derivative. Assuming $s_n(t)$ a continuous function, infinitely differentiable, lets note $s_n^{(i)}(t)$ the derivatives of $s_n(t)$ at the order i with respect to t :

$$s_n^{(2(i-1))}(t) = (-1)^{i-1} (\omega)^{2(i-1)} A_1 \sin(\omega t + \varphi_1) + \dots + (-1)^{i-1} (n\omega)^{2(i-1)} A_n \sin(n\omega t + \varphi_n) \quad (5)$$

All derivatives until order $2(n-1)$ give the system of equations:

$$\begin{pmatrix} 1 & \dots & 1 \\ -\omega^2 & & -(n\omega)^2 \\ \vdots & & \vdots \\ (-1)^{n-1} (\omega)^{2(n-1)} & \dots & (-1)^{n-1} (n\omega)^{2(n-1)} \end{pmatrix} \begin{pmatrix} A_1 \sin(\omega t + \varphi_1) \\ \vdots \\ A_n \sin(n\omega t + \varphi_n) \end{pmatrix} = \begin{pmatrix} s_n(t) - \bar{s} \\ s_n^{(2)}(t) \\ \vdots \\ s_n^{(2(n-1))}(t) \end{pmatrix} \quad (6)$$

The numerical solution of this system gives $A_i \sin(i\omega t + \varphi_i)$ as a linear combination of the elements of the $n+1$ dimensional vector $(\bar{s}, s_n(t), s_n^{(2)}(t), s_n^{(4)}(t), \dots, s_n^{(2(n-1))}(t))^T$.

Let \bar{r}_i and $r_{i,j}$ ($i = 1, \dots, n, j = 0, \dots, n-1$) be the coefficients of this combination:

$$A_i \sin(i\omega t + \varphi_i) = \bar{r}_i \bar{s} + \sum_{j=0}^{n-1} r_{i,j} s_n^{(2j)}(t) \quad (7)$$

By deriving equation (7), we obtain the expression of $A_i \cos(i\omega t + \varphi_i)$:

$$A_i \cos(i\omega t + \varphi_i) = \frac{\sum_{j=0}^{n-1} r_{i,j} s_n^{(2j+1)}(t)}{i\omega} \quad (8)$$

Replacing in the elements $A_i \sin(i\omega t + \varphi_i)$ and $A_i \cos(i\omega t + \varphi_i)$ by their expressions (7) and (8), give an expression of $s_n(t+\Delta t)$ according to the $2n+1$ dimensional vector :

$$S_n(t) = \left(\bar{s}, s_n(t), s_n^{(1)}(t), s_n^{(2)}(t), \dots, s_n^{(2(n-1))}(t), s_n^{(2n-1)}(t) \right)^T \quad (9)$$

Let a_{2i} ($i=1, \dots, 2n+1$) be the coefficients of this linear relation:

$$s_n(k+1) = s_n(t + \Delta t) = a_{2,1} \bar{s} + \sum_{j=2}^{2n+1} a_{2,j} s_n^{(j-2)}(t) = a_{2,1} \bar{s} + \sum_{j=2}^{2n+1} a_{2,j} s_n^{(j-2)}(k) \quad (10)$$

By derivative of equation:

$$s_n^{(1)}(t + \Delta t) = \omega A_1 \cos(\omega t + \varphi_1) \cos(\omega \Delta t) - \omega A_1 \sin(\omega t + \varphi_1) \sin(\omega \Delta t) + \dots + n\omega A_n \cos(n\omega t + \varphi_n) \cos(n\omega \Delta t) - n\omega A_n \sin(n\omega t + \varphi_n) \sin(n\omega \Delta t) \quad (11)$$

Replacing in the elements $A_i \sin(i\omega t + \varphi_i)$ and $A_i \cos(i\omega t + \varphi_i)$ by their expressions (7) and (8), give an expression of $s_n^{(1)}(t+\Delta t)$ as a function of vector $S_n(t)$ like in equation:

$$s_n^{(1)}(k+1) = s_n^{(1)}(t + \Delta t) = a_{3,1} \bar{s} + \sum_{j=2}^{2n+1} a_{3,j} s_n^{(j-2)}(t) = a_{3,1} \bar{s} + \sum_{j=2}^{2n+1} a_{3,j} s_n^{(j-2)}(k) \quad (12)$$

The same process can be repeat until $s_n^{(2n-1)}(t + \Delta t)$. Therefore, we build a set of linear relations corresponding to the state model (2).

$$\begin{cases} S_n(k+1) = \begin{pmatrix} \bar{s} \\ s_n(t + \Delta t) \\ s_n^{(1)}(t + \Delta t) \\ \vdots \\ s_n^{(2n-1)}(t + \Delta t) \end{pmatrix} = \begin{pmatrix} 1 & 0 & \dots & 0 \\ a_{2,1} & a_{2,2} & & a_{2,2n+1} \\ \vdots & & \ddots & \vdots \\ a_{2n+1,1} & \dots & \dots & a_{2n+1,2n+1} \end{pmatrix} \begin{pmatrix} \bar{s} \\ s_n(k) \\ s_n^{(1)}(k) \\ \vdots \\ s_n^{(2n-1)}(k) \end{pmatrix} + \zeta(k) \\ s_n(k) = (0 \ 1 \ 0 \ \dots \ 0) S_n(k) + \zeta(k) \end{cases} \quad (13)$$

Note that for the HSM of order n , the proposed state vector is $S_n(t)$, dimension $2n+1$, composed by the successive derivative of $s_n(t)$.

$$S_n(t) = \left(\bar{s}, s_n(t), s_n^{(1)}(t), \dots, s_n^{(2(n-1))}(t), s_n^{(2n-1)}(t) \right)^T \quad (14)$$

2.2.2 Computation of the transition matrix

The state equation of the HSM with order $(n+1)$ is:

$$S_{n+1}(t + \Delta t) = F_{n+1} S_{n+1}(k) + \zeta(k) \quad (15)$$

The transition matrix F_{n+1} can be directly calculated by solving system (6) written at order $(n+1)$, but can also be recursively determined from the transition matrix F_n of the harmonics state model of order n . In that case, calculations are simplified. Appendix details the method to compute F_{n+1} recursively from F_n .

2.2.3 Estimation of the state vector component

The estimate of the state vector of $S_n(t)$ the HSM model is obtained by means of a Kalman filter. Kalman filter is a recursive tool to estimate the state vector of a dynamic system from a distribution of observations (noisy measurements) and an evolution equation [30]. Kalman filter is a statistical approach and takes into account the uncertainty associated to the measurements. Using Kalman filter with HSM introduces the constraint of signal periodicity. Kalman filter only supposes the assumption of Gaussian distribution for noises.

The use of such filter is a way to limit the impact of the noise of the measures by realizing a second level of smoothing. The first level of smoothing results from the choice of model order. This both smoothing allows obtaining a modeling shape that conserves more than the characteristic points.

2.3 Point-to-point track

In section 2.2, we have explained all the theory around the construction of the model HSM and its application to a contour of the LV.

The model HSM is a local linear model which is represented by a state vector whose first elements are respectively the average value and the derivatives of the radius of a specific point in the contour at an angle θ . Thanks to the linearity of the model, all state vectors (at a selected order) of the contour may be determined by fixing the step of reconstruction (related to the number of points on the contour to be restored). The study of changes of signs on the matrix of vectors make it possible to find the position of characteristic points which are in a gradual way the extremums (cancellation of the first derivative), inflection points (cancellation of the second derivative), etc.

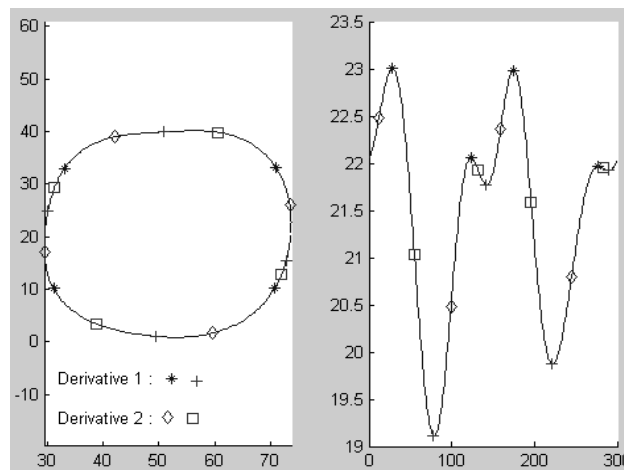


FIGURE 1: The positions of interest point at order 6 for two derivatives (1 and 2).

Thus, between two successive contours of the cardiac cycle which one knows the positions of characteristic points, we can establish a mapping. The risk of being misled by a change in the characteristic points and their positions is minimal given that the movement between two moments of the cardiac cycle is weak.

2.3.1 The mapping

The matching between two contours at successive moments is done in two stages. First of all, the connections are established between the characteristics points of the two contours. It is only after that the control points are connected based on the directions defined in the first step.

2.3.1.1 Mapping characteristic points

Characteristic points or points of interest are organized by groups in order to recognize whether the extremums maximum or minimum, a point of inflection entering or outgoing, etc. This helps to avoid connections between points of interest of different types. The reconstruction of the contour allows obtaining the state vectors of all points of the contour and these vectors are put together to constitute a matrix. The groups of points of interest are obtained through the study of derivatives of state vectors in this matrix. This study is equivalent to detect changes of signs in each column of the matrix. So in the end, we created two great sets of which the first brings together the points of passage of the positive sign to negative sign; and the second set contains all the crossing points of opposite signs. In each set, we have groups that agglomerate points from each column of the matrix. Obviously, the first two columns of the matrix are excluded from this work because they represent the average and the value of the radius, which are constant values. The establishment of groups will help to obtain a framed and fine match.

The application of method LCSS [31],[32],[33],[34] (Longest Common Sub-Sequence) with some constraints allows for the mapping of characteristic points. LCSS method is a dynamic mapping method that improves the DTW (Dynamic Time-Warping) method [35], [36]. It allows you to connect two temporal sequences with different sizes. We use it here, not in the timeframe, but space on sets whose values are not uniformly available in space. Contrary to the DTW, which puts all the points of departure of all in connection with the arrival points, the method LCSS does a match point to point by not establish more than one δ connection by point and limiting the search in a space defined by a threshold value δ .

The expressions defining the method LCSS for a threshold δ in a simplified version was made by Bahri [35] in (16).

Let A and B, two sets of values, the method LCSS is defined by the expressions below. In our case, sets of values (A and B) correspond to the indices of points of interest belonging to radius signal.

$$\left\{ \begin{array}{l} \text{LCSS}_\delta(A, \langle \rangle) = \text{LCSS}_\delta(\langle \rangle, B) = \text{LCSS}_\delta(\langle \rangle, \langle \rangle) = 0 \\ \text{LCSS}_\delta(A, B) = 1 + \text{LCSS}_\delta(\text{end}(A), \text{end}(B)) \\ \quad \text{if } |\text{last}(A) - \text{last}(B)| < \delta \\ \text{LCSS}_\delta(A, B) = \max(\text{LCSS}_\delta(\text{end}(A), B), \\ \quad \text{LCSS}_\delta(A, \text{end}(B))) \text{ if } |\text{last}(A) - \text{last}(B)| \geq \delta \end{array} \right. \quad (16)$$

With $\text{last}(A)$ the last element of sequence A and the $\text{rest}(A)$ all elements of A except the last.

The execution of the method is recursive and LCSS raises the construction of a table. The stages of LCSS for a typified representation table are described in (17). This is the table built to determine the points to put in connection. These points are obtained by determining the optimal path in the table, which way is found of the following specific steps. For two sets $A = \{a_i\} \ i=1, \dots, n$ and $B = \{b_j\} \ j=1, \dots, m$, with n the size of A and m the size of B, we note T the table holds values created by the LCSS_δ . All cases, $T(i, j)$, which pass through the optimal path puts in connection element i of A with element j of B. The readings of the path are:

1. Initialization of the trail on the last cell of the table $T(n, m)$;
2. From the case $T(i, j)$, if $|a_{i-1} - b_{j-1}| < \delta$ then we are going to establish a connection between the element a_i of A and b_j of B, and also a move to the case $T(i-1, j-1)$.
3. Otherwise, if $T(i, j-1) > T(i, j-1)$ then we move to the case $T(i, j-1)$, otherwise it is to the case $T(i-1, j)$.
4. Return to step 2 until reach case $T(1, .)$ or $T(., 1)$.

$$T(i, j) = \begin{cases} 0 & \text{if } i = 0 \text{ or } j = 0 \\ 1 + T(i-1, j-1) & \text{if } |a_i - b_j| < \delta \\ \max(T(i-1, j), T(i, j-1)) & \text{if } |a_i - b_j| \geq \delta \end{cases} \quad (17)$$

An example of application of LCSS, with and without threshold, will illustrate the method.

Two sets of values : $A=\{4,5,7,40,7,9,11\}$ and $B=\{3,5,6,7,10,12\}$
 Tables 1 and 2 represent the cumulative values of the LCSS without threshold and with threshold respectively. The boxes are framed on the optimal path:

		3	5	6	7	10	12
	0	0	0	0	0	0	0
4	0	1	1	1	1	1	1
5	0	1	2	2	2	2	2
7	0	1	2	3	3	3	3
40	0	1	2	3	4	4	4
7	0	1	2	3	4	5	5
9	0	1	2	3	4	5	6
11	0	1	2	3	4	5	6

TABLE 1: Table of LCSS without threshold

The optimal path of Table 1 will find that all the points are {5-3, 7-5, 40-6, 7-7, 9-10, 11-12}.

		3	5	6	7	10	12
	0	0	0	0	0	0	0
4	0	1	1	1	1	1	1
5	0	1	2	2	2	2	2
7	0	1	2	3	3	3	3
40	0	1	2	3	3	3	3
7	0	1	2	3	4	4	4
9	0	1	2	3	4	5	5
11	0	1	2	3	4	5	6

TABLE 2: Table of LCSS with threshold set to 10

Table 2, which is obtained by LCSS with value threshold of 10, has a different mapping result with the set of values {4-3, 5-5, 7-6, 7-7, 9-10, 11-12}.

The choice of the threshold value is very delicate. In defining the size of the search window, it plays on possible points of interest that can be mapped.

Once the mapping of intra-group points of interest carried out, we put them all in a single package. The merger of groups reflects a redundancy of information and some differences in the connections. A phase of post-processing is then carried out to overcome these minor problems.

The post-processing is done in three stages. First of all, the ordered fusion points of interest C_t which are matched to those of C_{t+1} is performed (Figure 3.1). This results in the elimination of isolated points of interest. The second step is in amalgamating the close points. This is reflected by the melting points of C_t or C_{t+1} are at a distance less than one parameter set. We preserve only the item on the average of small groups of points to merge (Figure 3.2). The third and final stage involves the cross-connections between points of interest. It includes such points p_i and p_j of C_t which are respectively connected to points of p_n and p_m of C_{t+1} . This step will restore order in the connections so that we have a liaison between p_i and p_n , but also between p_j and p_m (Figure 3.3). The post-treatment concluded this section on the matching of characteristic points.

2.3.1.2 Mapping of control points

Once the characteristic points, or at least what remains about it connected, we focus on the control points. It is a set of points positioned uniformly or not, on the outline start C_t and we will track their displacement on contour C_{t+1} . It is not necessary to track all points of the contour, since the control points give an estimate of the movement on the whole contour by the trajectories obtained. For connecting each control point P_b , linear interpolation is performed between the

points of the interval containing P_i , defined by two successive characteristic points of the contour C_t , and all points in the interval of their correspondents on contour C_{t+1} . And it only remains to find which points of C_{t+1} corresponds to P_i and the connection is established. We repeat this process for all checkpoints.

2.3.2 Algorithm

The steps involved in the process for tracking a set of control points (P_i) are shown in figure 2. The process of section 2.3 allows us to obtain trajectories covering the entire cardiac cycle. Figure 3 provides an overview of the matching between two contours. An additional modeling of these paths is done in order to have filtered trajectories where the effects of noise are eliminated.

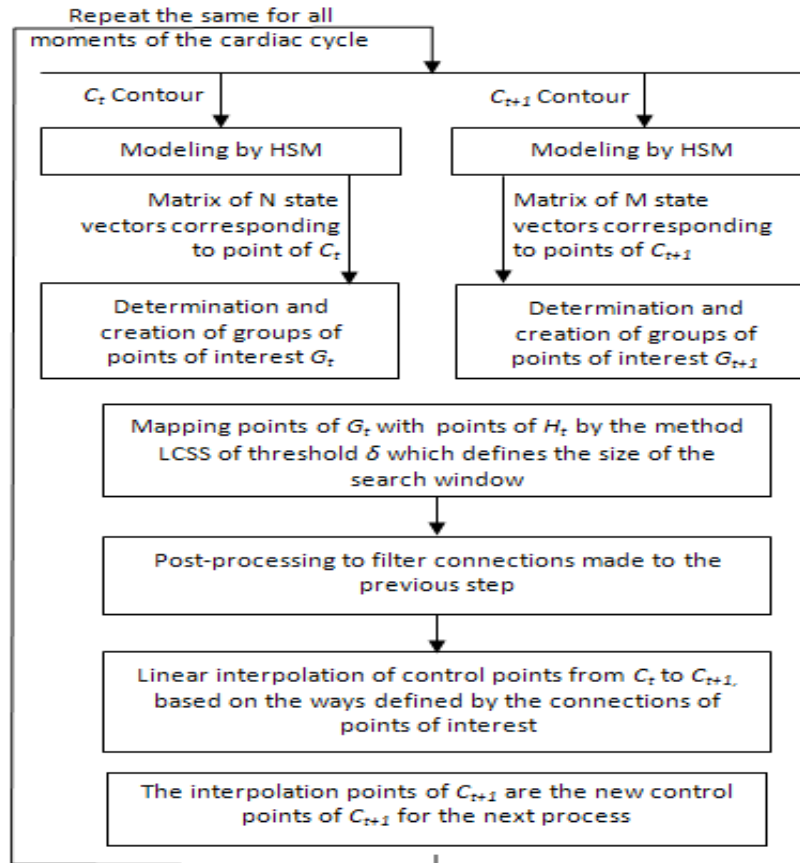


FIGURE 2: Process tracking of control point on the entire cardiac cycle

3. EXPERIMENTATION AND RESULTS

Throughout this section, the parameters of the tracking will be evaluated carefully. They are the best settings that will subsequently be implemented for the test phase on the shape of the cardiac cycle LV. Part of these contours is the result of clinical examinations images.

3.1 Parameters and post-processing

The elements involved in this tracking approach are studied and the values of various parameters set to obtain optimal results.

Here, we must provide answers to several questions such as the order of the model to use? What is the best size window of research? What is the criterion value for optimal fusion of characteristic points? and more others questions.

Because the tracking work is done on the contours of LV, which are strongly closed circular contours, a low order model was chosen, in occurrence order 4. This order is low enough to rebuild the contour in its general shape without any time to take again these small variations introduced by noise measurements and segmentation. This order also provides a consistent, but not excessive, characteristic points for each derivative. At the end, all derivatives are sufficient characteristic points to underline the important characteristics of the shape of contour.

The value threshold δ of the LCSS constitutes the size of the window mapping. The tests we have taken to the set at 20. The connection is then established under the best conditions and too great shifts are avoided.

During the post-treatment, a fusion operation of near points of interest is made. The parameter that defines the minimum proximity between two points is set at 4. Figure 3 provides an overview of the evolution of inter-connection points in the process of post-treatment.

In order to ensure a smooth interpolation that occurs just before the matching of control points, and after post-treatment, a generation of 300 points on the contours is necessary. Control points are 20 and are at equal angular distance on the contour of the first cycle.

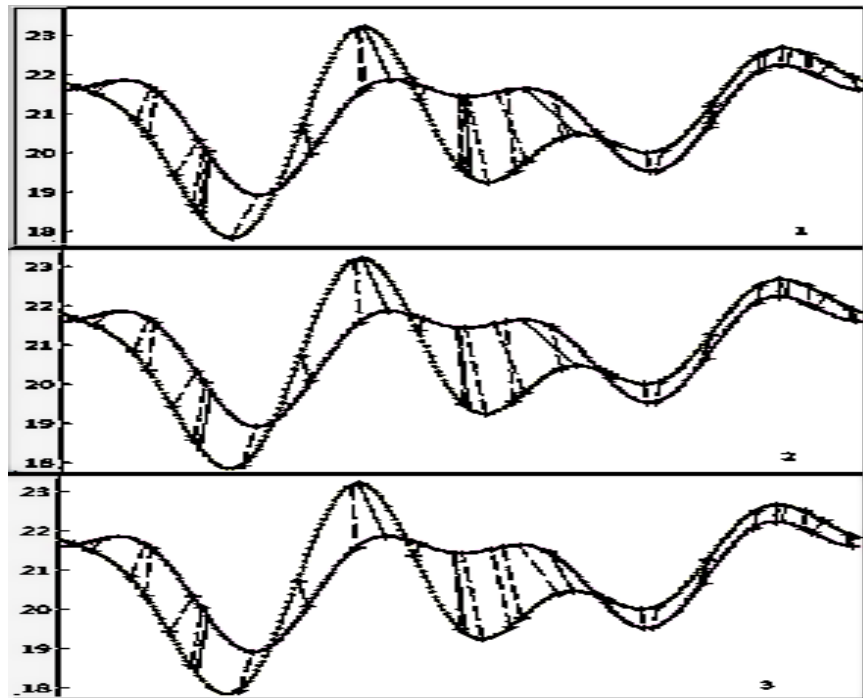


FIGURE 3: Results of the stages of post-treatment, the connectors in dotted lines are for characteristic points and the connectors in continuous lines are for control points.

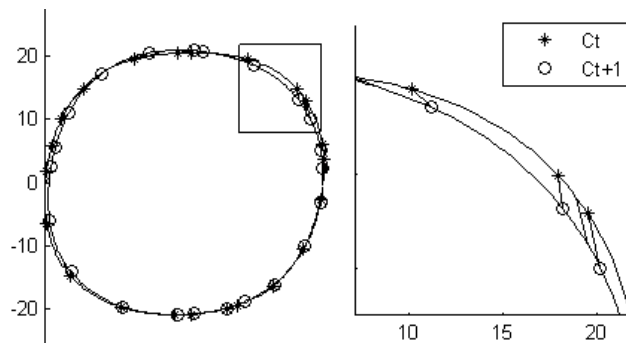


FIGURE 4: Position and correspondence between the interest points of C_t contour and those of C_{t+1} contour

3.2 Real data

The tracking work will be applied to real image sequences that are derived from clinical examinations.

3.2.1 Database

The works on actual data have been made on the basis of 3D+time cine-MRI¹ clinically validated. This database also contains the contours extracted from left ventricle conducted both by experts and by an automatic method [37]. This database is free to use and available to the public through the assistance of the Institut Gaspard-Monge and laboratory A2SI. The images are those of 18 patients with 25 or 22 images 3D per patient, covering the cardiac cycle. Each volume or 3D image contains an independent number of cuts (2D images), which is a function of resolution, hence no consistency between the volumes in this regard. These images, obtained from clinical examinations, are unfortunately not classified whatsoever to distinguish the types of diseases or simply to separate healthy patients from those whom are sick. However, the base remains a good support for the modeling and tracking 2D.

3.2.2 Evaluation of method on one patient

We apply our method for tracking 3D images of patient 4 and, specifically, cut at level 5. We thus have a set of 25 round contours covering the cardiac cycle and are approximately $\frac{1}{4}$ of the volume of the LV from the apex. Tracking is carried out for 20 points. Figure 6 shows the trajectories obtained for the outer contour (1) and internal (2). The trajectories modeled and filtered of these trajectories are found in Figure 6 (3, 4). We use HSM model to do it.

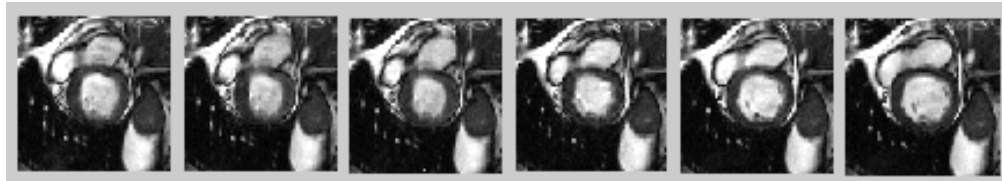


FIGURE 5: Some images of the 3D volumes (cut 5) for the patient 4

¹ 4D heart database : <http://www.laurentnajman.org/heart/>

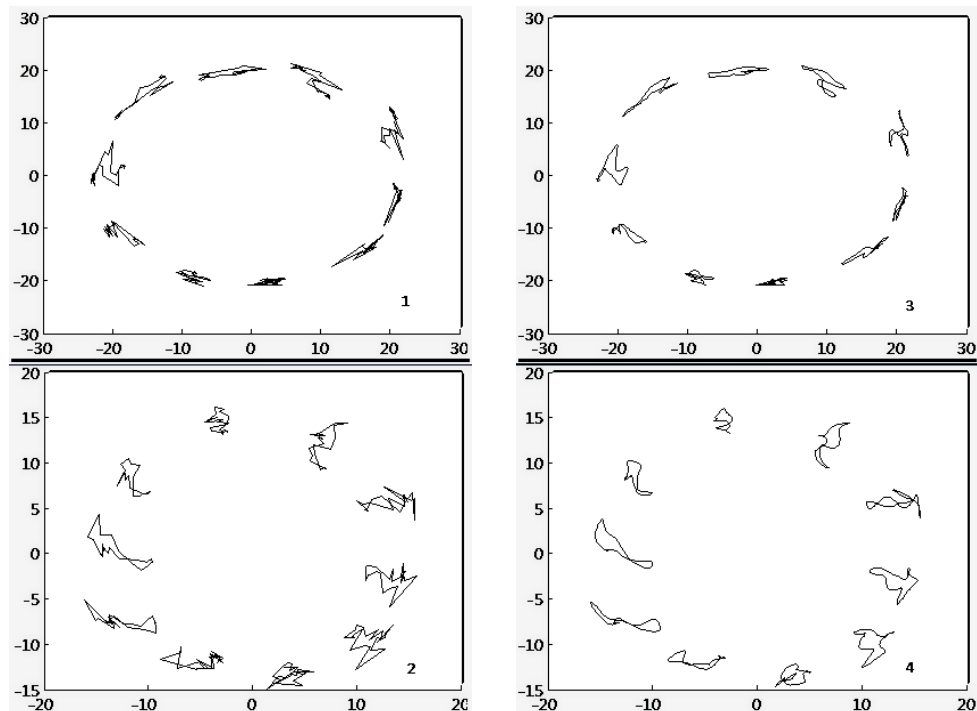


FIGURE 6: Trajectories of control points: (1) epicardium and (2) endocardium; modeled trajectories modeled by HSM model: (1) => (3) and (2) => (4).

We can notice in figure 6 that the trajectories have shapes that are consistent with the cardiac movements. The trajectories of the outer contour are more crushed than the internal contour, and this corresponds to the fact that the outer wall of the LV is more static than the inner wall. The collapse of the trajectories of the inferior part of the inner wall suggests a dysfunction of this part.

3.2.3 Trajectories and analysis of results

Thereafter, the implementation of the method is extended to the whole database. It focuses on both internal and external contours of the left ventricle. It is done by tracking the trajectories of 20 control points evenly distributed on each contour. The resulting information is aggregated into graphs (bull's eyes). These graphs provide the evolution of some parameters in time (throughout the cardiac cycle). The parameters are those which provide a direct interpretation of the movement of the myocardium. On this basis, it is possible to make a diagnosis on the state of the heart. These parameters are:

- The average variation of LV thickness;
- The speed of the endocardium (inner contour);
- The speed of the epicardium (outer contour).

To limit the size of calculations, the LV is divided into three equal parts along the long axis. The short axis cuts corresponding to the middle of each block could be tracked by computing their trajectories. These cuts represent the global movement made by the block where they belong. In the figures that follow, we present the results of three patients each with a different medical state:

- Healthy heart;
- Case reflecting a dyskinetic pathological;
- Case reflecting a hypokinetic pathological.

3.2.3.1 Details of graphs

For each figure, we have three lines that are in the midst of cutting long axis of LV. Each line consists of four graphs that represent the parameters vary during the cardiac cycle. We therefore, respectively (from left to right):

- Trajectories from inner and outer myocardium surfaces;
- The variation of the thickness of the myocardium (for each t , this is the difference between the thickness estimated by the model at t and the average thickness estimated by the same model);
- The variation of the speed of the inner radius (for each time t is the difference between the speed estimated by the model at time t and the value average speed estimated by the same model);
- The variation of the speed of the outer radius (for each time t is the difference between the speed estimated by the model at time t and the average speed estimated by the same model);

The graphs are bull's-eyes of parametric colored by the variations of parameters of each LV 20 regions. The direction of change is from inside to outside.

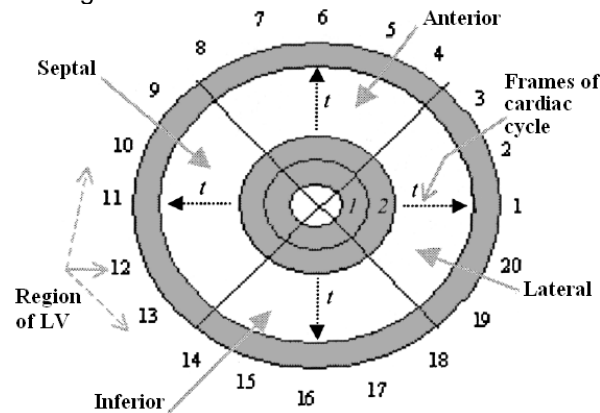


FIGURE 7: The LV is divided into 20 regions then grouped into 4 major regions. Each ring represents a frame cardiac cycle.

3.2.3.2 Analysis of graphs

FIGURE 8:

Graphs showing the variation in thickness have almost a uniform color on each ring (frame). The graphs, on third and fourth columns, show velocity variations remain uniformly circular. Speed variations are regular and not sharp on all regions of the LV. The movement is synchronous in all regions. We are therefore dealing with a heart healthy.

FIGURE 9:

For the three cuts, the variation in thickness of the myocardium is not uniform on the rings. Speed variations are very important with big change from one extreme to another. This applies to both internal and external radius. Then, the heart has a disordered contractile movement. We can conclude that it is a heart with dyskinetic pathology.

FIGURE 10:

For this patient, the trajectories have a small size, almost circular. These trajectories indicate a limited movement of the endocardium and the epicardium. The graphs of thickness variations confirm this observation, with a uniform color. Exceptions for two graphs of speed, these graphs show variations of low amplitudes. All this leads us to believe that we are in the case of a hypokinetic cardiac pathology or weak heart movement.

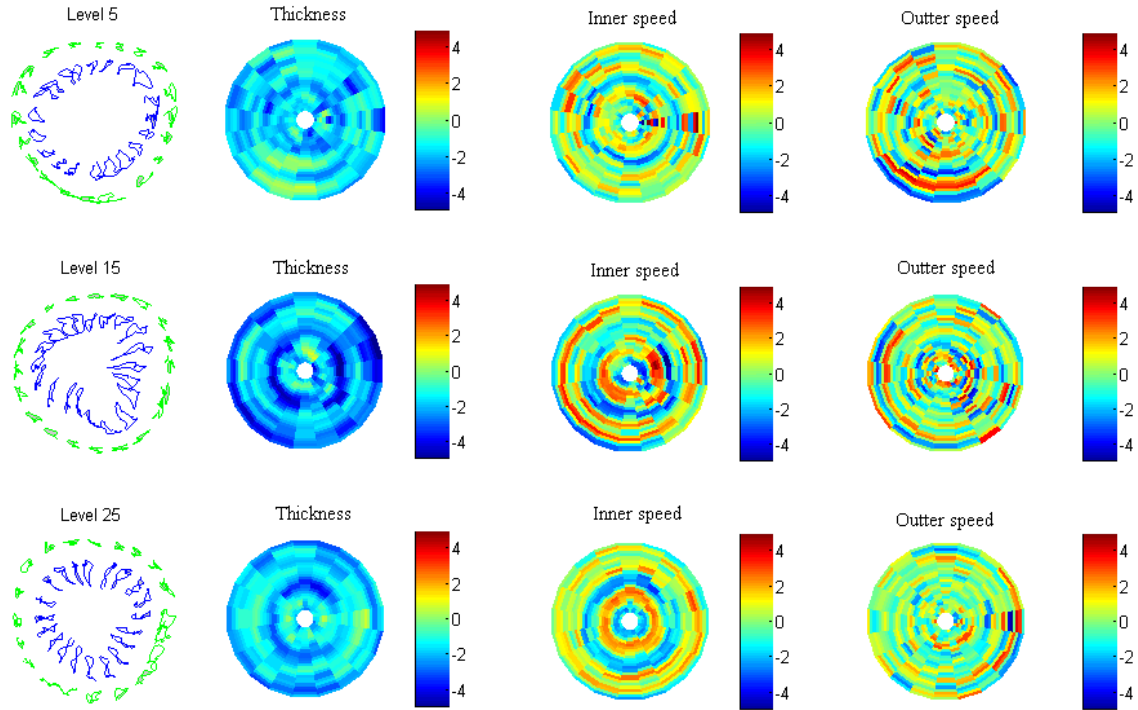


FIGURE 8: Graphs of parameters for a health heart (patient 8)

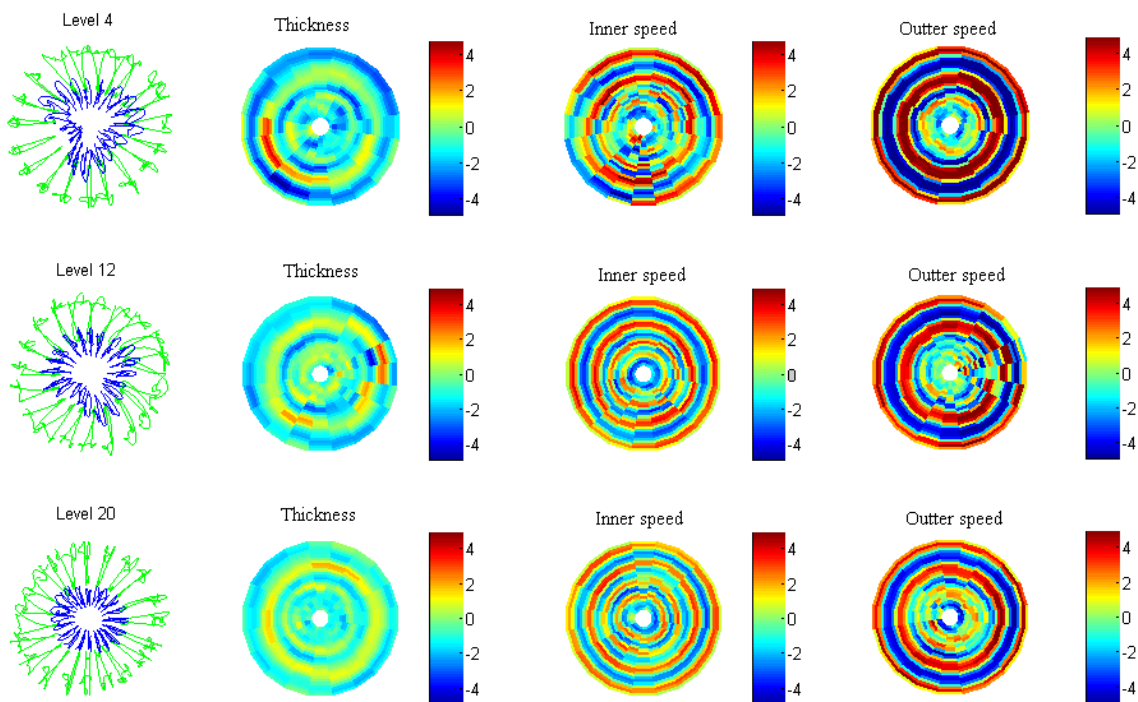


FIGURE 9: Graphs of parameters for a pathologic heart: dyskinetic (patient 6)

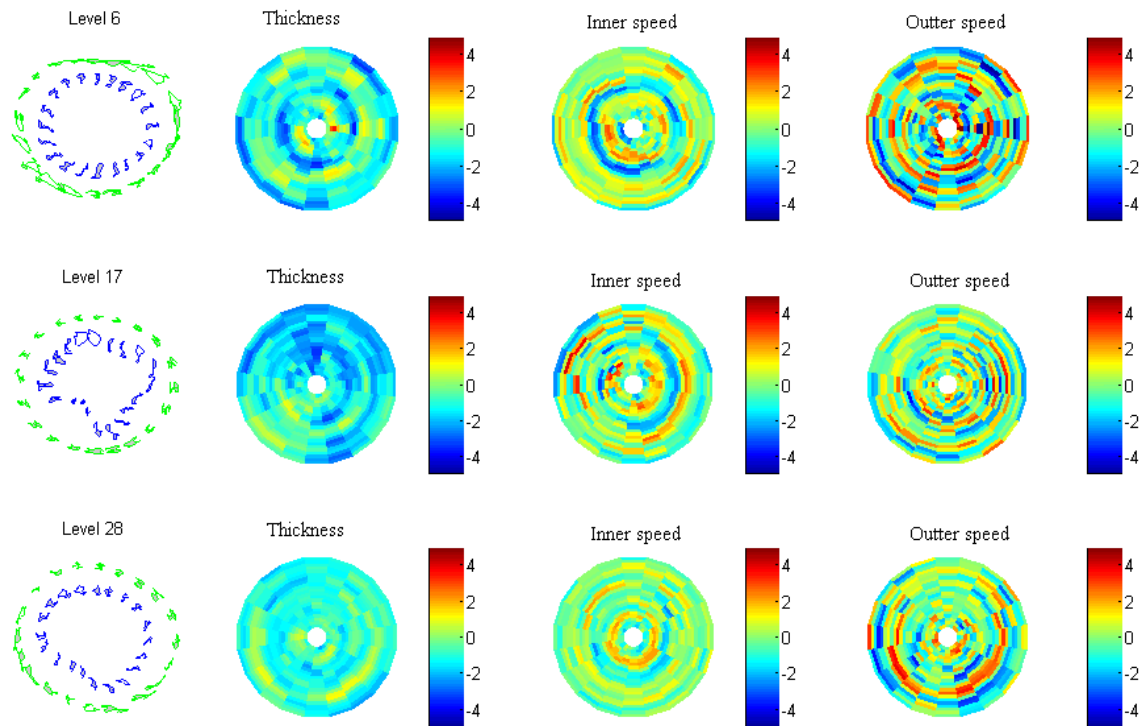


FIGURE 10: Graphs of parameters for a pathologic heart: hypokinetic (patient 13)

4. CONCLUSION & FUTURE WORK

In reviewing the dedicated literature, we have noted many approaches in achieving the modeling and tracking. An important point in tracking the movement of the LV is to make a judicious compromise between the quality of tracking and taking into account the specificities of the latter, as it contains information concerning its pump function. Based on the model of the HSM, we have carried out a 2D contour modeling of LV at each time cycle. Our approach exploits the spatial modeling of the model, which had not yet been made, and its resistance to noise. This model allows finding the characteristic points of the contour. The mapping of these points through the method LCSS and a post-processing allows building trajectories LV points throughout the cardiac cycle. In addition to the trajectories, we gain settings helping with the issue of diagnosis. The experimental results are lead on a base of real pictures provided by clinic exams. The analysis of various parameters generated from these images can provide guidance on the clinical status of patients. All three patients presented in this document are representative of the processing is done on all patients. Our method allows to easily and instantly distinguishing between heart disease and heart healthy through the issue of parameter and the reconstruction of trajectories.

The number of sequences with the actual base is limited and unclassified, we are thinking about moving to a stage of validation on a larger scale. This validation step, we will also make a comparison between our method and the best available technology as the method HARP [38] for MRI tagged.

The result of this work will be done on two main components: first, improving the layout of trajectories, thus improving accuracy, and then, and it is already the case, the application process on envelopes of greater dimensions.

5. REFERENCES

1. P.T. Buser, W. Auffermann, W.W. Holt, S. Wagner, B. Kirker, C. Wolfe, C.B. Higgins. "Non invasive evaluation of global left ventricular function with use of cine nuclear magnetic resonance". Journal of the American College of Cardiology 2(13) pp.1294-1300, 1989.
2. N.F. Osman and J.L. Prince. "Direct calculation of 2D components of myocardial strain using sinusoidal MR tagging". to appear in Proc. of the SPIE Medical Imaging: Image Processing Conference, San Diego, California, 1998.
3. E. McVeigh. "MRI of myocardial function: motion tracking techniques". Magnetic Resonance Imaging, 14(2):137-150, 1996.
4. J. C. Nascimento, João M. Sanches, Jorge S. Marques. "Tracking the Left Ventricle in Ultrasound Images Based on Total Variation Denoising". Proceedings of the 3rd Iberian conference on PRIA, Spain, pp. 628-636, 2007.
5. J. C. Nascimento and J. S. Marques. "Robust shape tracking in the presence of cluttered background". IEEE Trans. Multimedia, vol. 6, no. 6, pp. 852-861, 2004.
6. Chandra Sekhar Panda, Srikanta Patnaik, "Filtering Corrupted Image and Edge Detection in Restored Grayscale Image Using Derivative Filters", International Journal of Image Processing (IJIP), vol.3, issue 3, pp. 105-119, 2009.
7. M. Oumsis, A. D. Sdigui, B. Neyran et I.E. Magnin. "Modélisation et suivi par modèle d'état harmonique du mouvement ventriculaire gauche du cœur en Imagerie par Résonance Magnétique". Dans Traitement du Signal 2000 – volume 17 – n 5/6 – pages 501-516.
8. P. S. Hiremath, Jagadeesh Pujari. "Content Based Image Retrieval based on Color, Texture and Shape features using image and its complement", IJCSS, International journal of computer science and security, vol. 1, issue 4, pp. 25-35, Dec 2007.
9. Rajashree Shettar. "A Vertical Search Engine: based on Domain Classifier", Proceedings of International Journal of Computer Science and Security (IJCSS), vol. 2, issue 4, ISSN (Online): 1985-1553, pp. 18-27, Nov 2008.
10. P.L. Evina Ekombo, M. Oumsis, M. Meknassi, "A novel shape descriptor on both local and global curve properties using harmonic state model", IRECOS journal, July 2009.
11. M. Kass, A. Witkin, and D. Terzopoulos, "Snakes Active Contour Models". International Journal of Computer Vision, vol. 1, pp. 321-331, 1988.
12. T. F. Cootes, C. J. Taylor, D. H. Cooper, and J. Graham. "Active shape models: Their training and application". CVIU, 61(1):38-59, 1995.
13. J. Declerck, J. Feldmar, and N. Ayache. "Definition of a 4D continuous planispheric transformation for the tracking and the analysis of left-ventricle motion". Med. Image Anal., vol. 2, no. 2, pp. 197-213, 1998.
14. J. Huang, D. Abendschein, V. Davila-Roman, and A. Amini. "Spatio-temporal tracking of myocardial deformations with a 4-D B-spline model from tagged MRI". IEEE Trans. Med. Imag., vol. 18, no. 10, pp. 957-972, Oct. 1999.
15. P. J. Besl and N. D. McKay. "A method for registration of 3-D shapes". IEEE Transaction on Pattern Analysis and Machine Intelligence, 14(2):239-256, February 1992.

16. J. Declerck, J. Feldmar, N. Ayache. "Definition of a 4D continuous polar transformation for the tracking and the analysis of LV motion". INRIA. N° 3039, November 1996.
17. S. Benayoun, N. Ayache and I. Cohen. "An adaptive model for 2D and 3D dense non rigid motion computation". Technical report 2297, INRIA, May 1994.
18. M. Sühling, M. Arigovindan. "Myocardial Motion Analysis from B-Mode Echocar-diagrams". IEEE Transactions on image processing, vol. 4, April 2005.
19. M. J. Ledesma-Carbayo, J. Kybic, M. Desco, A. Santos and M. Unser. "Cardiac Motion Analysis from Ultrasound Sequences Using Non-rigid Registration". MICCAI 2001, pp. 889-896, 2001.
20. Sven Lončarić, Tvrtko Macan. "Point-constrained optical flow for LV motion detection". Proceeding SPIE, vol. 3978, 521, 2000.
21. A. Yilmaz, O. Javed, and M. Shah. "Object tracking: A survey". ACM Computer Survey, 38(4):13.1–13.45, 2006.
22. W. Sun, M. Cetin, R. Chan, V. Reddy, G. Holmvang, V. Chandar, A. Willsky. "Segmenting and Tracking the Left Ventricle by Learning the Dynamics in Cardiac Images". Lecture Notes in Computer Science, pp. 553-565 (2005).
23. M. P. Jolly. "Automatic segmentation of the left ventricles in cardiac MR and CT images." IJCV, 70(2):151–163, 2006.
24. W. Hong, B. Georgescu, X. S. Zhou, S. Krishnan, Y. Ma, and D. Comaniciu. "Database-guided simultaneous multi-slice 3D segmentation for volumetric data". ECCV, 4:397–409, 2006.
25. M. Dewan, C. H. Lorenz, and G. D. Hager. "Deformable motion tracking of cardiac structures (DEMOTRACS) for improved MR imaging". CVPR, 2007.
26. P. F. U. Gotardo, K. L. Boyer, J. Saltz, and S. V. Raman. "A new deformable model for boundary tracking in cardiac MRI and its application to the detection of intra-ventricular dyssynchrony". CVPR, 1:736–743, 2006.
27. Y. Wang, B. S. Peterson and L. H. Staib. "Shape-based 3D surface correspondence using geodesics and local geometry". In Proceedings of IEEE Conference on Computer Vision and Pattern Recognition, pp. 644-651, 2000.
28. X. Papademetris, J. Sunisas, Dione and Duncan. "Estimation of 3D left ventricular deformation from Echocardiography". Medical Image Analysis In Press, March 2001.
29. Geiger, Gupta, Costa, and Vlontzos. "Dynamic Programming for Detecting, Tracking and Matching Deformable Contours". IEEE Transactions PAMI 17(3)294-302, 1995.
30. R.E. Kalman. "A New Approach to Linear Filtering and Prediction Problems". Journal of Basic Engineering, pp. 35-45. March 1960.
31. Tae Sik Han, Seung-Kyu Ko, Jaewoo Kang. "Efficient Subsequence Matching Using the Longest Common Subsequence with a Dual Match Index". 5th International Conference on Machine Learning and Data Mining in Pattern Recognition (MLDM), Leipzig, Germany, July 18-20, 2007: 585-600.

32. M. Vlachos, G. Kollo, D. Gunopulos. *“Discovering Similar Multidimensional Trajectories”*. 18th IEEE Int. Conf. on Data Engineering (ICDE), pp.673-684, San Jose, USA 2002.
33. Haidar Siba. *“Comparaison des Documents Audiovisuels par Matrice de Similarité”*. PhD thesis, University of Toulouse III - Paul Sabatier, September 2005.
34. Xu Yuxiang; Dafang Zhang; Jiaohua Qin. *“An Improve Algorithm for the Longest Common Subsequence Problem”*. Convergence Information Technology, 2007. International Conference on Volume, Issue, 21-23, pp. 637–639, Nov. 2007.
35. Bahri A., Y. Naïja et G. Jomier. *“Recherche par similarité de séquences dans les bases de données: un état de l’art”*. Manifestation de JEunes Chercheurs STIC (MAJESTIC 2004), Calais, France, Octobre 2004.
36. R. Tavenard, L. Amsaleg, G. Gravier. *“Estimation de similarité entre séquences de descripteurs à l’aide de machines à vecteurs supports”*. Proc. Conf. Base de Données Avancées, Marseille, France, 2007.
37. J. Cousty, L. Najman, M. Couprie, S. Clément-Guimaudeau, T. Goissen, J. Garot. *“Automated, Accurate and Fast Segmentation of 4D Cardiac MR Images”*. Functional Imaging and Modeling of the Heart (2007), pp. 474-483
38. N.F. Osman and J.L. Prince. *“Direct calculation of 2D components of myocardial strain using sinusoidal MR tagging”*. In Proceeding of the SPIE Medical Imaging: Image Processing Conference, 1998, San Diego, California.

6. Appendix

Recursive estimation of transition matrix

The Fourier decomposition at order n is:

$$s_n(k) = s_n(t) = \bar{s} + A_1 \sin(\omega t + \varphi_1) + \dots + A_n \sin(n\omega t + \varphi_n) \quad (\text{A.1})$$

The SHM at the same order is:

$$S_n(k+1) = \begin{pmatrix} \bar{s} \\ s_n(t + \Delta t) \\ s'_n(t + \Delta t) \\ \vdots \\ s_n^{(2n-1)}(t + \Delta t) \end{pmatrix} = F_n \begin{pmatrix} \bar{s} \\ s_n(k) \\ s'_n(k) \\ \vdots \\ s_n^{(2n-1)}(k) \end{pmatrix} + \zeta(k) \quad (\text{A.2})$$

With

$$F_n = \begin{pmatrix} 1 & 0 & \dots & 0 \\ a_{2,1} & a_{2,2} & & a_{2,2n+1} \\ \vdots & & \ddots & \vdots \\ a_{2n+1,1} & \dots & \dots & a_{2n+1,2n+1} \end{pmatrix} \quad (\text{A.3})$$

The Fourier decomposition at order $n+1$ is:

$$s_{n+1}(t) = s_n(t) + s_{n+1}^*(t) \quad (\text{A.4})$$

With

$$s_{n+1}^*(t) = A_{n+1} \sin((n+1)\omega t + \varphi_{n+1}) \tag{A.5}$$

A state form of this harmonic is given by:

$$\begin{aligned} \begin{pmatrix} s_{n+1}^*(t + \Delta t) \\ s_{n+1}^{*'}(t + \Delta t) \end{pmatrix} &= \begin{pmatrix} \cos((n+1)\omega \Delta t) & \frac{\sin((n+1)\omega \Delta t)}{(n+1)\omega} \\ -(n+1)\omega \sin(i\omega \Delta t) & \cos((n+1)\omega \Delta t) \end{pmatrix} \begin{pmatrix} s_{n+1}^*(t) \\ s_{n+1}^{*'}(t) \end{pmatrix} \\ &= \mathbf{\alpha}_i \begin{pmatrix} s_{n+1}^*(t) \\ s_{n+1}^{*'}(t) \end{pmatrix} \end{aligned} \tag{A.6}$$

We want to obtain the SHM at order $(n+1)$:

$$\begin{pmatrix} \bar{s} \\ s_{n+1}(k+1) \\ s_{n+1}^{(1)}(k+1) \\ \vdots \\ s_{n+1}^{(2n+1)}(k+1) \end{pmatrix} = F_{n+1} \begin{pmatrix} \bar{s} \\ s_{n+1}(k) \\ s_{n+1}^{(1)}(k) \\ \vdots \\ s_{n+1}^{(2n+1)}(k) \end{pmatrix} + \zeta(k) \tag{A.7}$$

Equation (6) written at order $n+1$ gives:

$$\begin{pmatrix} 1 & \dots & 1 \\ -\omega^2 & & -((n+1)\omega)^2 \\ \vdots & & \vdots \\ (-1)^n & \dots & (-1)^n (n\omega)^{2n} \end{pmatrix} \begin{pmatrix} A_1 \sin(\omega t + \varphi_1) \\ \vdots \\ A_{n+1} \sin((n+1)\omega t + \varphi_{n+1}) \end{pmatrix} = \begin{pmatrix} s_{n+1}(t) - \bar{s} \\ s_{n+1}^{(2)}(t) \\ \vdots \\ s_{n+1}^{(2n)}(t) \end{pmatrix} \tag{A.8}$$

By mean of upper triangularization (numerical solution), the last component of the harmonic decomposition is:

$$\begin{aligned} s_{n+1}^*(t) &= A_{n+1} \sin((n+1)\omega t + \varphi_{n+1}) \\ &= \bar{r}_{n+1} \bar{s} + \sum_{j=0}^n r_{n+1,j} s_{n+1}^{(2j)}(t) \end{aligned} \tag{A.9}$$

By derivation:

$$s_{n+1}^{*'}(t) = \sum_{j=0}^n r_{n+1,j} s_{n+1}^{(2j+1)}(t) \tag{A.10}$$

From Equations (A.4) and (A.9):

$$\begin{aligned} s_n(t) &= s_{n+1}(t) - s_{n+1}^*(t) \\ &= s_{n+1}(t) - \bar{r}_{n+1} \bar{s} - \sum_{j=0}^n r_{n+1,j} s_{n+1}^{(2j)}(t) \end{aligned} \tag{A.11}$$

And derivation of order $2i$:

$$s_n^{(2i)}(t) = s_{n+1}^{(2i)}(t) - (-1)^i ((n+1)\omega)^{2i} A_{n+1} \sin((n+1)\omega t + \varphi_{n+1}) \tag{A.12}$$

$$s_n^{(2i)}(t) = s_{n+1}^{(2i)}(t) - (-1)^i ((n+1)\omega)^{2i} \left[\bar{r}_{n+1} \bar{s} + \sum_{j=0}^n r_{n+1,j} s_{n+1}^{(2j)}(t) \right] \quad (\text{A.13})$$

By derivation

$$s_n^{(2i+1)}(t) = s_{n+1}^{(2i+1)}(t) - (-1)^i ((n+1)\omega)^{2i} \left[\sum_{j=0}^n r_{n+1,j} s_{n+1}^{(2j+1)}(t) \right] \quad (\text{A.14})$$

By writing Equation (A.4) at $t + \Delta t$

$$s_{n+1}(t + \Delta t) = s_n(t + \Delta t) + s_{n+1}^*(t + \Delta t) \quad (\text{A.15})$$

HSM at order n gives:

$$s_n(t + \Delta t) = a_{2,1} \bar{s} + \sum_{j=0}^{2n-1} a_{2,j+2} s_n^{(j)}(t) \quad (\text{A.16})$$

Equation (A.6) gives

$$s_{n+1}^*(t + \Delta t) = \cos((n+1)\omega \Delta t) s_{n+1}^*(t) + \frac{\sin((n+1)\omega \Delta t)}{(n+1)\omega} s_{n+1}^{*'}(t) \quad (\text{A.17})$$

Replacing in equation (A.15):

$$s_{n+1}(t + \Delta t) = a_{2,1} \bar{s} + \sum_{j=0}^{2n-1} a_{2,j+2} s_n^{(j)}(t) + \cos((n+1)\omega \Delta t) s_{n+1}^*(t) + \frac{\sin((n+1)\omega \Delta t)}{(n+1)\omega} s_{n+1}^{*'}(t) \quad (\text{A.18})$$

Replacing $s_n^{(j)}$ (A.13, A.14), $s_{n+1}^*(t)$ (A.5) and $s_{n+1}^{*'}(t)$ (A.10) by their expression, we obtain equation (A.19):

$$\begin{aligned} s_{n+1}(t + \Delta t) = & \left(a_{2,1} + \bar{r}_{n+1} \left(\cos((n+1)\omega \Delta t) + \sum_{i=1}^n a_{2,2i} \left((-1)^{(i)} ((n+1)\omega)^{2(i-1)} \right) \right) \right) \bar{s} + \\ & + \sum_{j=0}^{n-1} \left(a_{2,2(j+1)} + \cos((n+1)\omega \Delta t) r_{n+1,j} + r_{n+1,j} \sum_{i=1}^n a_{2,2i} \left((-1)^{(i)} ((n+1)\omega)^{2(i-1)} \right) \right) s_{n+1}^{(2j)}(t) \\ & + \sum_{j=0}^{n-1} \left(a_{2,2(j+1)+1} + \frac{\sin((n+1)\omega \Delta t)}{(n+1)\omega} r_{n+1,j} + r_{n+1,j} \sum_{i=1}^n a_{2,2i+1} \left((-1)^{(i)} ((n+1)\omega)^{2(i-1)} \right) \right) s_{n+1}^{(2j+1)}(t) \\ & + \left(a_{2,2(n+1)} + \cos((n+1)\omega \Delta t) r_{n+1,n} + r_{n+1,n} \sum_{i=1}^n a_{2,2i} \left((-1)^{(i)} ((n+1)\omega)^{2(i-1)} \right) \right) s_{n+1}^{(2n)}(t) \\ & + \left(a_{2,2(n+1)+1} + \frac{\sin((n+1)\omega \Delta t)}{(n+1)\omega} r_{n+1,n} + r_{n+1,n} \sum_{i=1}^n a_{2,2i+1} \left((-1)^{(i)} ((n+1)\omega)^{2(i-1)} \right) \right) s_{n+1}^{(2n+1)}(t) \end{aligned} \quad (\text{A.19})$$

This expression gives the second line of the matrix F_{n+1} . The expressions $s_{n+1}^{(i)}(t + \Delta t)$ are calculated by derivation of equation (A.19) with respect to Δt . In conclusion we have determined the coefficients connecting the vector $s_{n+1}^{(i)}(t + \Delta t)$ to the vector $s_{n+1}^{(i)}(t)$. These coefficients constitute the elements of the transition matrix F_{n+1} .